Highest-Speed Modulators Enabling High-Capacity Free Space Optical Communications at Low SNR

Laurenz Kulmer, Yannik Horst, Bertold Ian Bitachon, Marcel Destraz, Tobias Blatter, Matthieu Rimlinger, Aurélie Montmerle-Bonnefois, Joseph Montri, Caroline B. Lim, Jean-Marc Conan, Beatrice Sorrente, Nicolas Védrenne, Loann Pommarel, Daniel Matter, Benedikt Baeuerle, and Juerg Leuthold, *Fellow, IEEE*

(Top-Scored Paper)

***Abstract*—Free-space optical satellite-earth links often operate at the SNR limit. We show that under low SNR conditions it is more favorable to operate at higher speeds with lower order modulation formats. This follows from the Shannon capacity limit formula where the transmission bandwidth has a linear impact, whereas the SNR has a logarithmic effect. In practice, bandwidth limitations from the hardware need to be considered making capacity maximization a joint optimization. Here we experimentally substantiate these findings by e.g., comparing two 128 Gbit/s signals - encoded either as DP 64 GBd 2 PAM or a DP 32 GBd 4 PAM signal. It is found that the 64 GBd 2 PAM performs better for the same bit-error rate. To facilitate highest speed operation we employ a packaged plasmonic modulator with a 3 dB bandwidth $>$ 110 GHz. The plasmonic modulator also enabled us to send up to 160 GBd 2 PAM signals, achieving to the best of our knowledge the highest symbol rate in any free-space optical communication link. Reaching an achievable information rate of 276 Gbit/s. Even higher rates of 424 Gbit/s were achieved by employing a DP 128 GBd 4 PAM signal. This shows that once hardware bandwidth limitations come in place it is more favorable to increase the modulation complexity. Furthermore, we have shown that plasmonic organic hybrid modulators can withstand space radiation with only minor degradations. Lastly, the conditions during the experiment have been investigated and have been shown to constitute a worst-case scenario for earth-GEO feeder links.**

***Index Terms*—Adaptive optics, Earth-satellite communication, Electrooptic modulators, Free-space optical communication, Plasmonics, Silicon photonics, Turbulent atmospheric optical channel.**

Manuscript received 6 September 2023; revised 18 December 2023, 6 February 2024, and 15 March 2024; accepted 22 March 2024. Date of publication 28 March 2024; date of current version 16 May 2024. This paragraph of the first footnote will contain the date on which you submitted your paper for review. This work was supported by the H2020 EU Project VERTIGO under Grant 822030. *(Corresponding author: Laurenz Kulmer.)*

Laurenz Kulmer, Yannik Horst, Tobias Blatter, Matthieu Rimlinger, and Juerg Leuthold are with the Institute of Electromagnetic Fields (IEF) ETH Zurich, 8092 Zurich, Switzerland (e-mail: laurenz.kulmer@ief.ee.ethz.ch; yannik.horst@ief.ee.ethz.ch; tobias.blatter@ief.ee.ethz.ch; matthieu.rimlinger@inf.ethz.ch; leuthold@ethz.ch).

Bertold Ian Bitachon is with the Institute of Electromagnetic Fields (IEF) ETH Zurich, 8092 Zurich, Switzerland, and also with the Spiden AG, 8808 Pfaeffikon, Switzerland (e-mail: bertold.bitachon@ief.ee.ethz.ch).

Marcel Destraz and Benedikt Baeuerle are with the Polariton Technologies AG, 8134 Adliswill, Switzerland (e-mail: benedikt@polariton.ch; marcel.destraz@polariton.ch).

Aurélie Montmerle-Bonnefois, Joseph Montri, Jean-Marc Conan, Beatrice Sorrente, and Nicolas Védrenne are with the ONERA, DOTA, Paris Saclay University, F-92322 Châtillon, France (e-mail: aurelie.bonnefois@onera.fr; joseph.montri@onera.fr; jean-marc.conan@onera.fr; beatrice.sorrente@onera.fr; nicolas.vedrenne@onera.fr).

Caroline B. Lim was with the ONERA, DOTA, Paris Saclay University, F-92322 Châtillon, France.. She is now with the LNE-SYRTE, Observatoire de Paris, CNRS, Sorbonne Université, 75014 Paris, France (e-mail: caroline.lim@obspm.fr).

Loann Pommarel and Daniel Matter are with the Thales Alenia Space in Switzerland, 8052 Zurich, Switzerland (e-mail: loann.pommarel@thalesaleniaspace.com; daniel.matter@thalesaleniaspace.com).

Color versions of one or more figures in this article are available at https://doi.org/10.1109/JLT.2024.3382629.

Digital Object Identifier 10.1109/JLT.2024.3382629

I. Introduction

EARTH-SATELLITE links are promising candidates in many applications ranging from enabling internet access to rural areas as well as providing highest speed interconnects for satellites [1], [2]. In recent years, optical systems in earth-satellite-like links have been shown to offer higher capacity per second than RF links [1], [2], [3], [4], [5]. It may be envisioned that free-space-optical (FSO) networks linking space with terrestrial communication are the logical next step, see Fig. 1(a). Due to the maturity of fiber optical communication technologies, developing costs as well as time for future space systems should be low [2], [4]. This includes size, weight, and power consumption (SWAP) which is one of the scarcest resources in space. As those links are neither limited by dispersion nor suffer from the nonlinear Shannon limit, they are an ideal candidate for operation at highest speeds, only being limited by existing equipment [6].

Over the past years many different FSO transmission links have already demonstrated single carrier line rates of 10 Gbit/s and above in different transmission scenarios [4], [5], [7], [8], [9], [10], [11], [12], [13], [14], [15]. Single carrier line rates of 800 Gbit/s were demonstrated at distances of 42 m. Similarly, for Intra-datacenter scenarios a link of up to 1 Tbit/s over a distance of 3m was shown. Furthermore deploying 54 channels with an average line rate of 243 Gbit/s [11] demonstrated a 13.16 Tbit/s link over a distance of 10.45 km. Recently parts of this consortium, for the first time, demonstrated Tbit/s single carrier line rates over a link distance of 53.42 km [5]. Emulating worst-case GEO feeder links with highest capacity.

Yet, some main challenges remain in satellite-satellite and earth-satellite FSO communication channels. First, high link

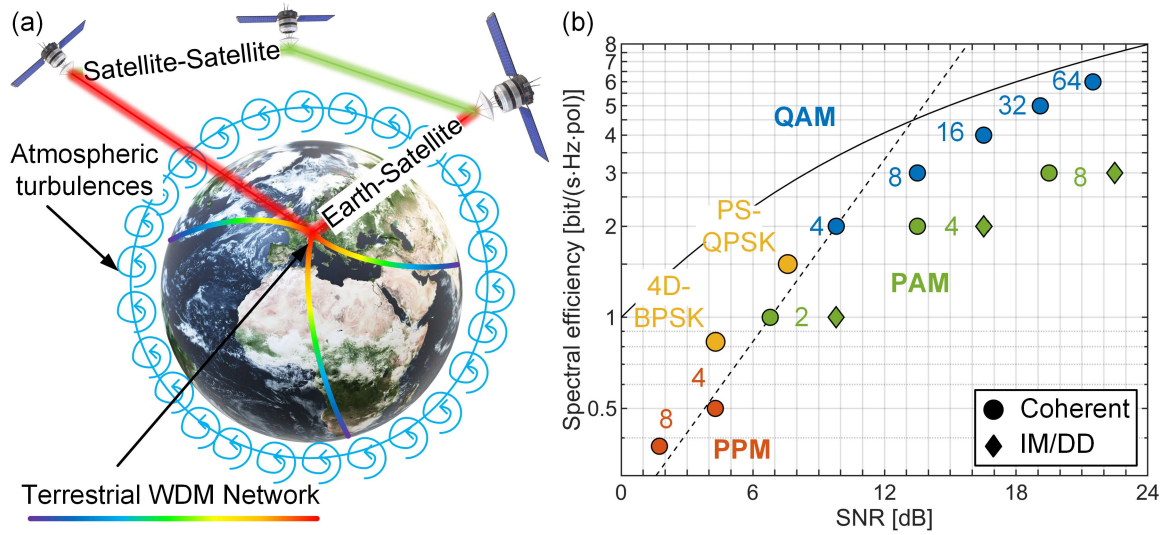

Fig. 1. (a) Schematic drawing of a free-space optical (FSO) communication system interconnecting earth and satellites. The terrestrial WDM network is shown in rainbow colors. Earth-to-satellite links are shown in red and satellite-to-satellite links are depicted in green. Atmospheric turbulences which affect the earth-to-satellite links are shown as blue spirals around the globe. (b) Spectral efficiency (SE) as a function of SNR for different modulation formats. Transitioning from one modulation format to another along the dashed line, the SE is increased by the same amount as the SNR requirement increase. Transitioning to modulation formats to the right of the dashed line comes at the price of a net SNR penalty. Transitioning to the left comes with a net SNR gain.

losses have to be overcome which is in part due to the long distances of around ∼38'000 km between satellite and ground station [16]. To overcome these losses and improve the signal-to-noise ratio (SNR), telescopes in the order of a few tens of centimeters are currently deployed [3], [16]. Due to the small size of the optical wavelength a couple of centimeters seem to be small, but they still offer better gain compared to their bigger RF counterparts [17], [18]. Current development on higher power amplifiers as well as interleaving also reduces the burden on telescope size requirements [19], [20]. Second, earth-satellite links face another challenge in atmospheric turbulences which distort the wavefront and induce power fluctuations. This hinders operation at a constant signal quality [19], although this problem can be in part mitigated by different techniques such as multi aperture reception [14], [19], [21], [22], adaptive optics (AO) [5], [18], [19], [23], [24], [25], [26], or highest FEC codings [19], [27], [28], [29]. Nonetheless, there will still be time-dependent power variations on the signal leading to low SNR values [25]. Hence, despite all these efforts earth-satellite links will always operate at the lower SNR limit – particularly when aiming at highest capacity.

One solution to improve the SNR issue can be derived from Fig. 1(b). The plot shows spectral efficiency versus the SNR. There is a trend to increase the capacity by transitioning to modulation formats with a higher spectral efficiency [30]. For instance, the community is moving from the simple BPSK modulation format with 1 bit/s/polarization to QPSK with 2 bit/s/polarization. This way the capacity indeed increases by a factor of 2 per transmitted symbol. Yet, the plot also shows that there is an SNR penalty of 3 dB to be paid. In essence, one has a factor of 3 dB in capacity but loses a factor 3 dB in SNR. Thus there is no net gain. The plot then shows the capacity gain versus the SNR penalty for each modulation format. It becomes clear that transitioning to the right of the dashed line is a solution to increase the capacity per symbol – yet it always comes at an SNR penalty. Transitioning to the modulation formats to the left of the dashed line will result in a net SNR gain. It should be stressed that unlike in fiber-based systems, this SNR gain can be realized as there is no nonlinear-Shannon limit (and therefore no peak-power constraint) in free space. Nonetheless, there will still be external power limitations in FSO systems such as eye safety regulations and availability of high-power amplifiers. Lastly, taking advantage of the SNR gain while keeping the capacity high comes at the price of components operating at higher bandwidth (as the spectral efficiency tends to be lower).

In this paper we show that there is a power advantage for operating space communications systems at higher symbol rates over applying higher order modulation formats – provided that higher speed components are available. Here we therefore employ plasmonic components for data encoding as they offer bandwidths in excess of 110 GHz [31]. We successfully demonstrate FSO transmission over a 53 km turbulent link with up to 160 GBd. As a key result we show a 1.8 dB advantage in received optical power when transmitting 128 Gbit/s with DP 64 GBd 2 PAM rather than transmitting at DP 32 GBd 4 PAM. Likewise, we show that a 128 GBd dual-polarized (DP) 4 PAM signal achieving an achievable information rate of 424 Gbit/s outperforms a 64 GBd DP 8 PAM signal with a net data rate of 338 Gbit/s. Yet, 4 PAM is superior to 2 PAM as our transmitter would need to operate beyond its bandwidth limits. In addition it is shown that the plasmonic modulators can withstand space radiation with only minor degradation. This makes them an ideal candidate for future space missions due to the low SWAP.

The paper is organized as follows. Section II details the setup of the used system and describes the terrain of the outdoor demonstration. Section III presents the obtained results in terms of rate per power as well as the highest achieved rates. Section IV focuses on the conclusion of the obtained results.

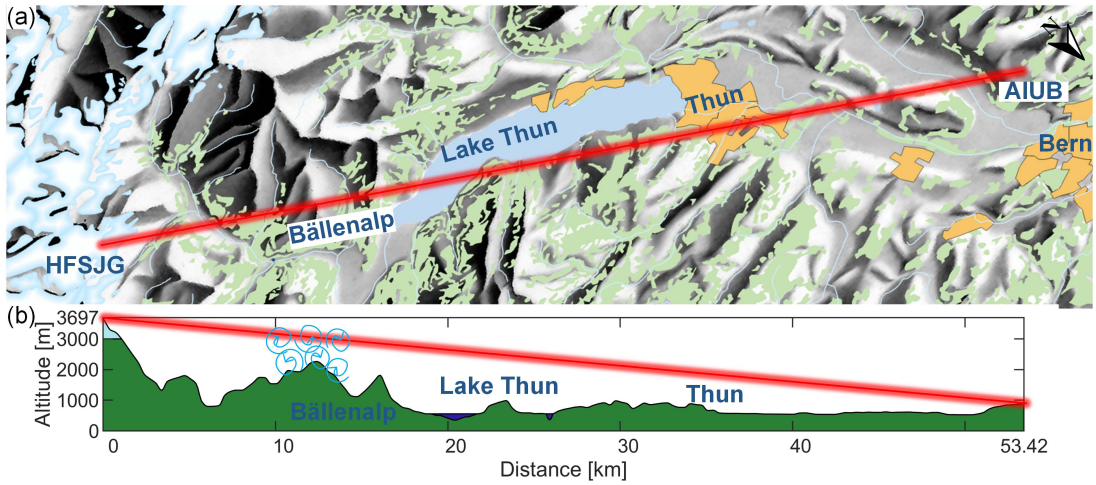

Fig. 2. (a) Location of the outdoor demonstration with important landmarks. The terrain is shown in different colors, glaciers, forests, lakes, cities as well as the relief are distinguishable. (b) Altitude over distance is shown. Map data as well as elevation profile was obtained from swisstopo.

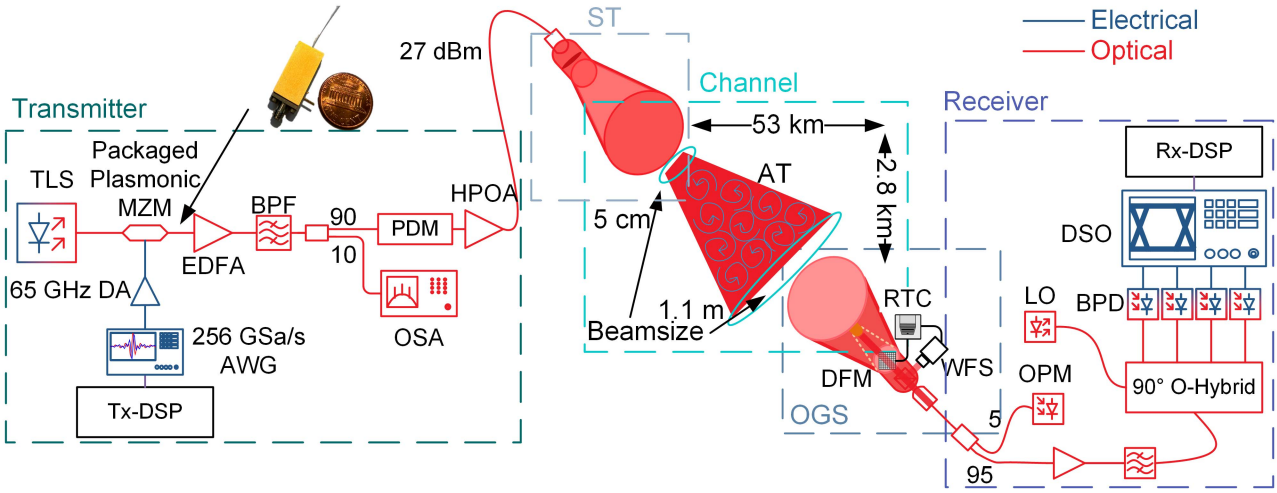

Fig. 3. Details the used setup. The setup is split into 5 parts, the transmitter, the space terminal (ST), the channel, the optical ground station (OGS), and the receiver. First, the signal waveform is generated by an offline transmitter digital-signal processing software (Tx-DSP). A tunable laser source (TLS) at 1550 nm is directly fed to the packaged plasmonic Mach-Zehnder-modulator (MZM) where the modulated signal which was generated by an arbitrary waveform generator (AWG) and amplified by a driving amplifier (DA). After the data is encoded into the optical domain, the signal is amplified by an erbium-doped-fiber amplifier (EDFA) before being filtered by an optical bandpass filter (BPF) and then polarization multiplexed (PDM). The signal is then amplified by a high-power-optical amplifier (HPOA) and transmitted through the free space link. The beam-sizes at the ST and OGS after/before the telescopes (red cones) are also indicated in the figure. The optical signal is received by a deformable mirror (DFM) which is controlled by a real-time-computer which is processing the feedback from a wavefront sensor (WFS). The optical signal is then coupled to a fiber where it is amplified in two stages, filtered, and then passed to an optical Hybrid (O-Hybrid) where the signal is mixed with a local oscillator (LO) and consequently downmixed by balanced photodetectors (BPD). The electrical signal is sampled by a digital-storage-oscilloscope (DSO) before being evaluated by the offline receiver DSP (Rx-DSP).

The content of the paper is an extended version of results first presented at the Optical Fiber Communications (OFC) conference 2023 [32].

II. Experimental Configuration

Fig. 3 shows the experimental setup of the used system in detail. While Fig. 2 details the geographical location of the outdoor demonstration. The bandwidths of some of the important system elements are shown in Fig. 4.

The FSO link spanned a distance of 53.42 km starting at the optical-ground-station (OGS) at the Jungfraujoch East Ridge in the Swiss Alps (approximately 3700 m above sea-level) to the space-terminal (ST) located at the Zimmerwald Observatory of the University of Bern, Switzerland (895 m above sea-level). The altitude difference results in an elevation loss of 2805 m. Due to the fact that the optical beam stays within the first turbulent atmospheric layer, this constitutes a worst-case scenario for an earth-satellite link [23]. This can also be seen in Fig. 2 as the depicted red beam, not just stays low to the ground but also propagates over cities, mountains, lakes, and glaciers causing all different thermal situations.

The experimental setup with the transmitter, ST, FSO channel, OGS, and the receiver are shown in detail in Fig. 3.

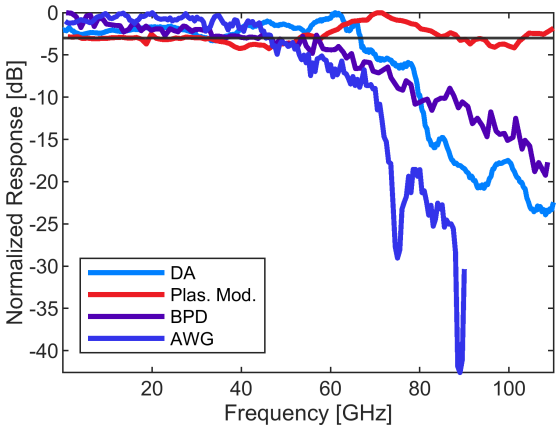

Fig. 4. Measured bandwidth of individual components of the communication system. Driving amplifier (DA), plasmonic modulator (Plas. Mod.), balanced photodetectors (BPD) as well as arbitrary waveform generator (AWG) are shown. The packaged Plasmonic modulator exhibits a 3 dB bandwidth in excess of 110 GHz.

The key enablers of this link are the high-speed plasmonic Mach-Zehnder-modulator (MZM), the AO system as well as the low-noise-amplifier (LNA) optical coherent receiver front-end. At the transmitter an offline digital signal processing (DSP) unit generates the digital waveform which is sent to a 256 GSa/s arbitrary-waveform generator (AWG) with an analog bandwidth of 70 GHz. The digital signal consists of bi-polar M-PAM signals for M = 2, 4, or 8. This is further amplified by a driving amplifier (DA) with a bandwidth of 65 GHz. The frequency response of the AWG and DA can individually be seen in Fig. 4. The electrical signal then propagates to a packaged plasmonic MZM, see bandwidth in Fig. 4. The plasmonic modulator is being fed by a laser at 1550 nm. The MZM is operated in the null point leading to a bipolar-amplitude modulation (PAM). After the first amplification stage the out-of-band noise of the signal is filtered by a 2 nm bandpass filter. The signal is then sent to a polarization division multiplexer (PDM) emulated by a split-and-delay architecture before being sent to a high-power-optical amplifier (HPOA). After amplification of the signal to output powers of up to 27 dBm it is transmitted to the ST with a sub-aperture of 4.2 cm for propagation in free space.

After the transmission through the 53.42 km link, which is detailed in Fig. 2, the optical beam is received by an OGS consisting of a telescope with an aperture of 35 cm and an AO system. The AO system consists of a deformable mirror (DFM) which is controlled by a real-time computer (RTC). The RTC is operated by a wavefront sensor (WFS) and the frequency of the control loop is 1.5 kHz. The WFS consists of an 8x8 Shack Hartmann sensor. The coherence time of the 53 km channel was measured to be in the order of milliseconds. The signal is then coupled back into a standard single-mode fiber. 95% of the incoming light is then brought to a low-noise amplifier. The remaining portion is sent to an optical power meter (OPM) in order to record the power fluctuations of the coupled power. The amplified signal is then filtered by an optical-bandpass filter before being amplified and again filtered. In a dual-polarized 90° optical hybrid (90 O-Hybrid) the amplified and filtered signal is combined with a local oscillator (LO) also operating at 1550 nm. The output signals were fed to four balanced photodetectors (BPD) for optical-to-electrical conversion. The electrical signal was then sampled by a digital storage oscilloscope (DSO). The DSO records a sequence lasting ∼15 µs. As this is roughly two orders of magnitude slower compared to the atmospheric turbulences, the turbulences and hence the power are assumed constant within one measurement. The digital signal is then processed by an offline DSP consisting of a matched filter, timing recovery, a 2x2 blind polarization demultiplexer, a carrier recovery followed by a 2x2 T/2-spaced feedforward least-mean square algorithm as well as a Volterra equalizer followed by a one sample per symbol-based feedforward least-mean square algorithm and symbol decision.

III. Experimental Results

In this section we describe the achieved information rates using the plasmonic modulator. First, keeping the line rate fixed at 128 Gbit/s but alternating the symbol rates, a comparison between a 64 GBd 2 PAM signal and a 32 GBd 4 PAM signal is done. Then, the highest performance of the presented link is investigated. We further show that plasmonic modulators can withstand space radiation. Lastly, the scintillation profile of the time horizon of the measurements is shown.

A. Low Order Modulation Format At Highest Speed to Transmit At Highest Capacity: 128 Gbit/s – 2 PAM Outperforms 4 PAM

Keeping the line rate fixed at 128 Gbit/s a comparison between a DP 64 GBd 2 PAM signal and a DP 32 GBd 4 PAM signal was performed. Line rates were obtained by multiplying the number of polarizations with the symbol rate as well as $\log_2(M)$, where M represents the order of the amplitude modulation. These points are also visualized in Fig. 6(a1-a2). The corresponding bit error rate (BER) over received optical power (ROP) can be seen in Fig. 5(a). One can clearly see that the 64 GBd signal has better performance compared to the 32 GBd signal. For a fixed BER the 64 GBd signal needs ∼1.8 dB less received optical power (ROP) compared to the 32 GBd signal. This is in agreement with the plot in Fig. 1(b) where we would also predict an SNR advantage (an SNR advantage of ∼3dB). Due to the low ROP the first amplifier will add more noise by amplified spontaneous emission to the system, leading to an overall worse SNR.

The advantage of lower order modulation formats becomes even more evident when looking at the effective net data rates. Effective net data rates are obtained by multiplying the line rate times FEC code rate times the outage probability. Outage probabilities can be calculated by dividing the number of occurrences where the normalized general mutual information (NGMI) drops below the needed NGMI threshold over the given measurement time. As in this case both signals are operated close to an NGMI of 1, a FEC overhead of 5.8% with an NGMI threshold of 0.987 [33] was chosen. This results in an outage probability of 2% for the 64 GBd 2 PAM signal and 12 % for the 32 GBd 4 PAM signal. This then yields an effective net data rate of 123.8 Gbit/s for the 2 PAM signal and 111 Gbit/s for the 4 PAM signal.

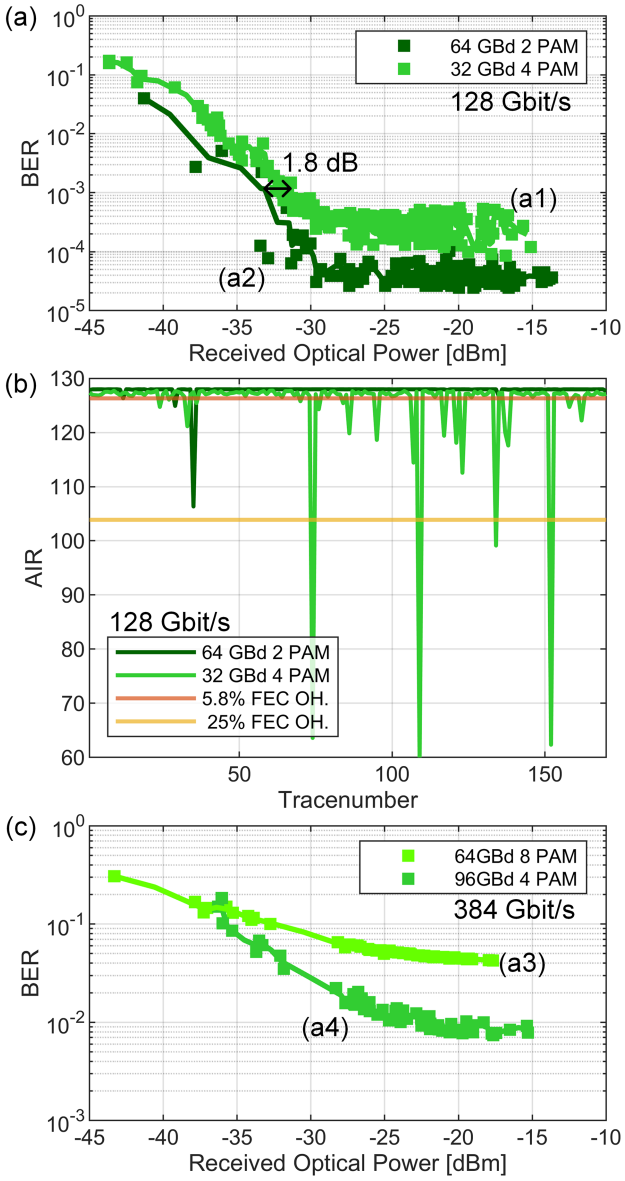

Fig. 5. (a) Comparison of BER as a function of received optical power (ROP) at a fixed line rate of 128 Gbit/s, points (a1, a2) in Fig. 6. The 64 GBd 2 PAM signal outperforms the 32 GBd 4 PAM signal. It can be seen that at low ROP (leading to lower SNR values), the 64 GBd signal outperforms the 32 GBd signal by around 1.8 dB. (b) Achievable information rates over 170 traces are given for the two 128 Gbit/s signals. One can see that the 2 PAM signal led to less outage time compared to the 4 PAM signal. Two FEC overheads corresponding to an overhead of 5.8% and 25% are visualized. (c) Comparison of BER as a function of ROP at a fixed line rate of 384 Gbit/s, points (a3, a4) in Fig. 6. Due to system limitations both signals operate at high BER and no fair point for comparison in terms of ROP can be reached. (OH. - overhead).

Using the same FEC threshold as discussed in section III.B the outage probabilities for the 2 PAM signal become 0% and 3.5% for the 4 PAM signal during this measurement. Resulting in an effective net data rate of 96.2 Gbit/s and 92.9 Gbit/s respectively. This is visualized in Fig. 5(b) where the achievable information rate (AIR) for the two 128 Gbit/s is plotted over 170 traces. As offline DSP was used, 170 traces were recorded over a timeframe of 255 s. In this time window the scintillation index was 1.6 and the Fried's coherence length was 5.8 cm on average, constituting

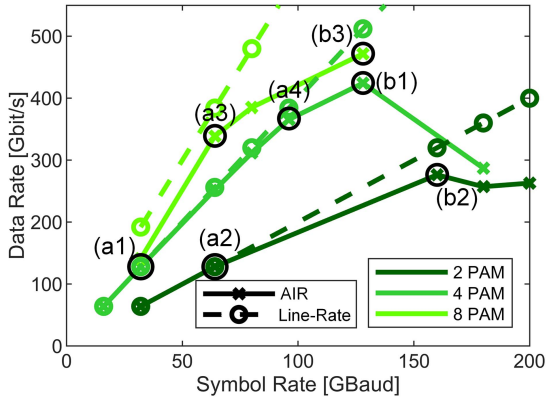

Fig. 6. Achievable information rates (AIR) as well as line rates for dual-polarized 2 PAM, 4 PAM, and 8 PAM signals as a function of the symbol rate. The data points reaching highest AIR for the respective modulation format while staying within a 25% FEC limit, are highlighted with (a3, b1, and b2). The points marked with (a1 and a2 as well as a3 and a4) both share the same line rate and are used for a fixed line rate comparison in section III.A. Point (b3) highlights the overall highest achieved information rate, however, its NGMI does not stay below the 25% FEC limit and is used for discussion in section III.B.

a worst-case scenario as stated in section III.D. The two NGMI thresholds were multiplied by the line rate of 128 Gbit/s and are also shown in Fig. 5(b). The achievable information rate (AIR) was calculated by multiplying the symbol rate with the generalized mutual information (GMI) per polarization.

A similar performance can be made by comparing the BER for points (a3) and (a4) in Fig. 6 with a constant line rate of 384 Gbit/s. The corresponding BER over ROP is plotted in Fig. 5(b). One can clearly see that the 96 GBd 4 PAM outperforms the 64 GBd 8 PAM. However, we refrain from comparing the two points here as the BER is too high to reach a fair point for comparison. In our setup we would find ROP advantages for symbol rates of up to 96 GBd. Beyond the bandwidth limitations of the used AWG, DA, and BPD start degrading the system performance. This is evident by looking at Fig. 6 and comparing the points with a line rate of 320 Gbit/s – namely the 160 GBd 2 PAM and the 80 GBd 4 PAM. As of this point it is beneficial to lower the symbol rate in order to transmit more data by increasing the modulation format.

B. Higher Order Modulation Format Under System Bandwidth Limitations – 4 PAM Outperforms 8 PAM and 2 PAM

Fig. 6 plots the highest achieved information rate as well as line rates as a function of symbol rates and used modulation format. These values represent best-case data rates for each modulation format. While all measurements were taken on the same day, received optical power values ranged between -50 to -13 dBm. The highest rate within the 25% FEC overhead [33] was achieved by employing a DP 128 GBd 4 PAM signal reaching an AIR of 424 Gbit/s, see point (b1) in Fig. 6. Operating the transmitter at a lower data rate with a DP 64 GBd 8 PAM signal we achieved an AIR of 338 Gbit/s, see point (a3).

It should be noted, that while the 8 PAM results with symbol rates higher than 64 GBd show a higher AIR, their NGMI

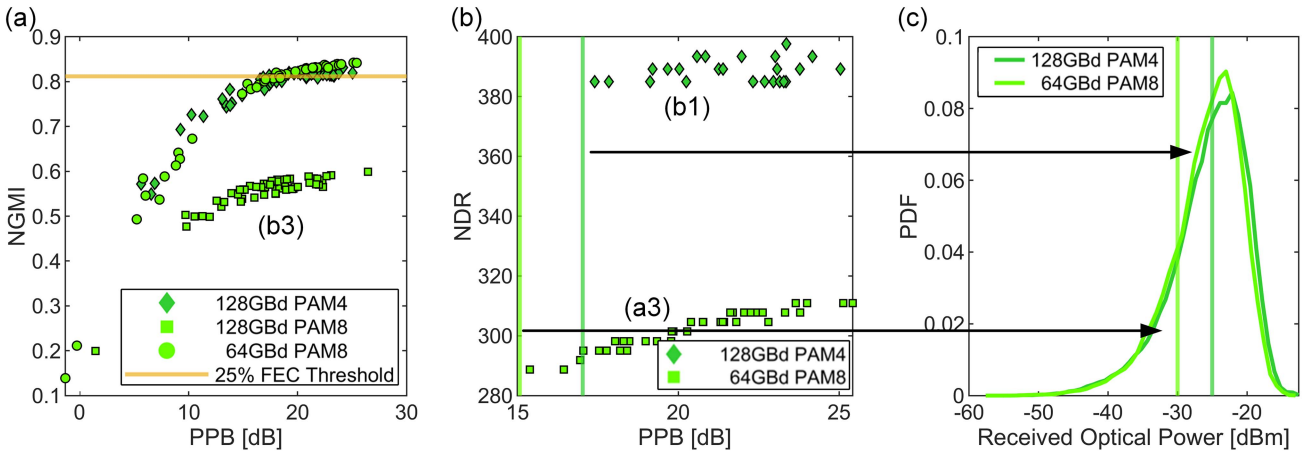

Fig. 7. (a) Normalized general mutual information (NGMI) over photons per bit (PPB) for points (a1), (b1), and (b3) of Fig. 6. As the shown signals, exhibit different line rates, PPB was chosen as a metric rather than received optical power (ROP). (b) Net-data rate (NDR) as a function of PPB. NDR was calculated by taking the calculated NGMI values from (a) combined with the FEC limits stated in [33] to calculate the NDR dependent on the achieved NGMI. The Two vertical lines correspond to the threshold where no points above the 25% threshold were measured. (c) The probability distribution function of the ROP. The ROP limits for the stated 25% FEC are again plotted for the two signals. Due to the lower line rate, the 64 GBd 8 PAM signal can communicate at lower power levels.

dropped below the chosen 25% FEC threshold and no comparison for those points is therefore carried out.

This although the received optical power for the 128 GBd 8 PAM at -13.6 dBm is significantly higher, when compared to the received power of -18.5 dBm for the 128 GBd 4 PAM signal. The difference stems from the time varying FSO channel with slightly better conditions during the recording of the 8 PAM signal. The NGMI over photons per bit (PPB) for points (a3), (b1) and (b3) is shown in Fig. 7(a). To adjust for the different line rates present in these points, PPB was chosen instead of ROP. PPB can be calculated by taking the number of incoming photons and dividing it by the line rate of the corresponding signal. In Fig. 7(b) net-data rates for the points above the 25%FEC threshold were calculated. Two vertical lines are also shown to indicate the points below which no points above the threshold were recorded anymore. In Fig. 7(c) the probability density function of the ROP is shown together with the observed power levels below which no point was above the FEC limit. From Fig. 7(c) it becomes evident that the 64 GBd 8 PAM signal can communicate more reliably compared to the 128 GBd 4 PAM signal. From this, one can again calculate an effective net-data rate. The outage probability for the 4 PAM signals lies at 44% while the outage probability of the 8 PAM signals comes out at 18%. Multiplying this with the respective line rates of 512 Gbit/s and 384 Gbit/s yields effective net-data rates of 237 Gbit/s and 216 Gbit/s respectively. The better reliability of the 384 Gbit/s 8 PAM signal compared to the 512 Gbit/s 4 PAM signal stems from the difference in line rate. As has already been shown in III.A, 4 PAM offers better reliability when the line rate is fixed. This shows that while highest AIR is wanted from a performance side, outage probabilities of employed system have to be accounted for.

When using a DP 160 GBd 2 PAM signal an AIR of 276 Gbit/s was achieved, see point (b2). The lower AIR is due to the fact that our transmitter was bandwidth limited – as outlined in Fig. 4. The eye diagrams of the three mentioned highest AIR are shown in Fig. 8 .

C. Space Qualification Tests

Some of the most important space qualification tests include vibration & shock tests, radiation tests, heat cycling, vacuum test as well as acoustic tests. In order to take a first step to assess the suitability of plasmonic organic hybrid (POH) [34] modulators for space applications radiation hardness tests with total ionization doses (TID) of up to 50 krad (Si) were performed. The tests were performed on unpackaged, unpassivated devices. These dose values are representative for typical LEO and GEO orbits, as investigated in satellite mission simulations with 10-year duration and Al shielding thicknesses below 5 mm using the AE-8, AP-8 and SHIELDOSE-2 models [35], [36] in SPENVIS [37]. Dose-independent, low changes in the order of 0.5 dB V_π (in line with results from [38]) were observed over the considered bandwidth of 70 GHz, see Fig. 3(c). This value represents a maximum degradation due to space radiation as the samples were not passivated and part of the effect might be due to ambient exposure.

Recently plasmonic modulators have also been shown to work at different temperatures, hence no heat cycling tests are shown here [39], [40].

D. Investigation of Atmospheric Turbulences

The presented measurements were conducted in a time period of 6 hours. During this measurement time, different atmospheric conditions were observed. Here, the measured Scintillation index (SI) and the Fried coherence length (also called the Fried parameter) r_0 are investigated as figure of merits to assess the encountered atmospheric turbulence conditions [41].

The *SI* is defined as the ratio of the standard deviation of the intensity σ_I to the average intensity of the beam *I*. These values were calculated based on the beam's intensity $I(x, y, t)$ in the pupil plane measured by the Shack-Hartmann WFS. The calculated values can be seen in Fig. 10(a). During this measurement timeframe the SI ranged between 1 and 2.2.

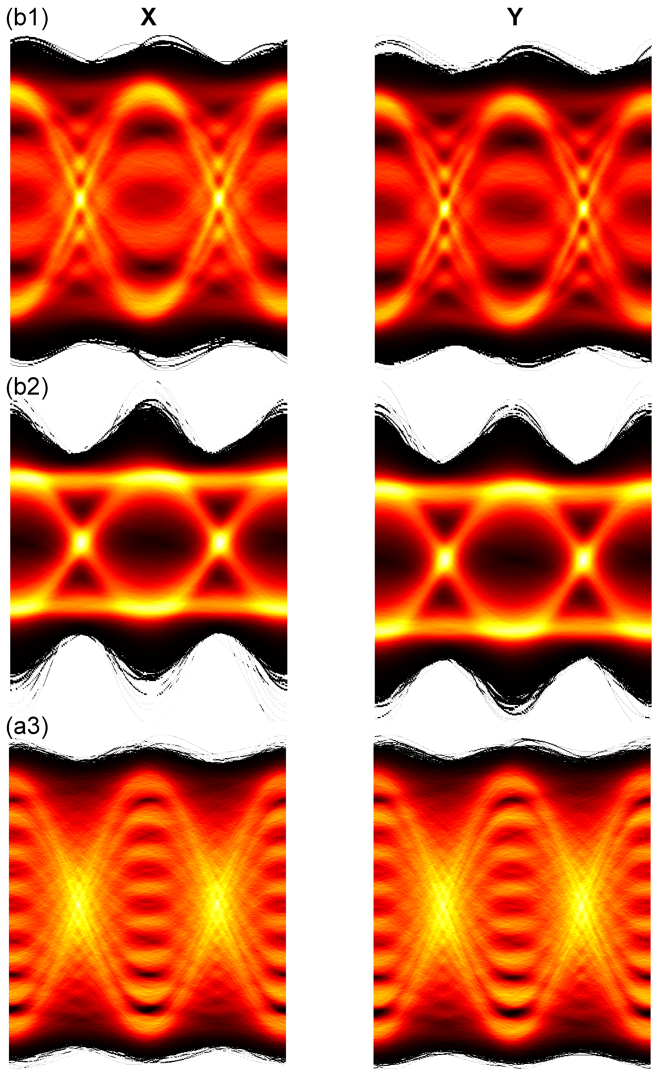

Fig. 8. Recorded eye diagrams for (b2) DP 160 GBd 2 PAM signal (b1) DP 128 GBd 4 PAM signal and (a3) DP 64 GBd 8 PAM signal. The two polarizations are shown independently and are labeled by **X** and **Y**.

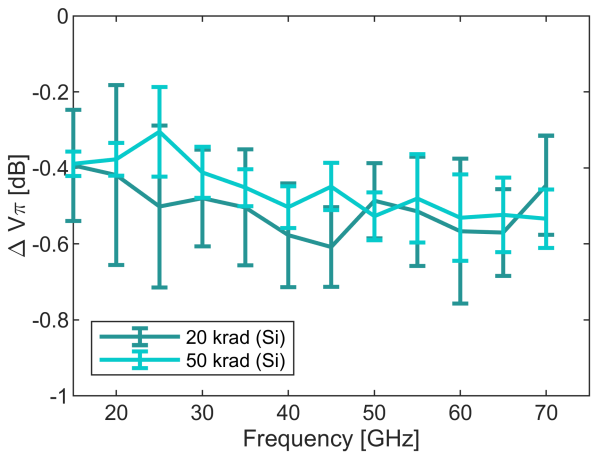

Fig. 9. Change in V_π over frequency after different TID. Unpackaged and unpassivated plasmonic modulators were exposed to a TID of 20 or 50 krad (SI). Later the difference in electro optic modulation efficiency was measured. A dose independent reduction around 0.5 dB was measured.

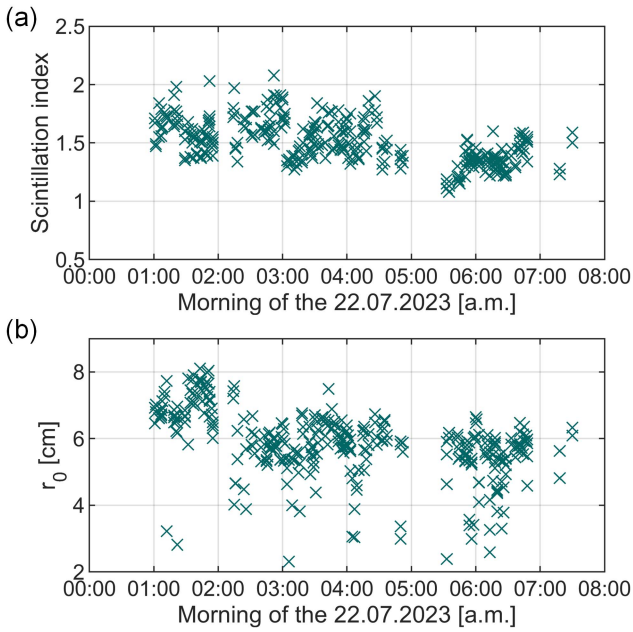

Fig. 10. Measured Scintillation Index (a) as well as Fried's coherence length (b) over the measurement time horizon.

This represents above average bad conditions, as SI-values in GEO-earth links are typically $\ll 1$ [18]. Even under very high turbulent conditions the SI typically does not exceed 1. The Fried's coherence length r_0 describes the phase spatial correlation of the EM wave [41]. Therefore, strong turbulence-induced phase variations result in a small r_0. It is estimated through post-processing of AO data (Shack-Hartmann data and DFM commands) [18], [42]. For earth-GEO transmission scenarios, values in the order of $r_0 \sim 4$ cm are expected [18]. As can be seen in Fig. 10(b) estimated values range in the order between 2 and 8 and are therefore comparable to the values that would be observed in an actual earth-GEO transmission scenario.

IV. Conclusion

Free-space optical links often operate under low SNR conditions. We have shown that for free-space communications it is favorable to use lower order modulation formats at higher speeds rather than lower-speed communications with higher order modulation formats. This holds for systems that are not hardware bandwidth limited. The result is supported by a transmission experiment over a 53 km turbulent link. When comparing two signals each with a line rate of 128 Gbit/s, a DP 64 GBd 2 PAM signal provides a 1.8 dB advantage in received-optical power over a DP 32 GBd 4 PAM signal.

Once hardware bandwidth limitations come into effect, it is preferable to sacrifice speed in order to increase the AIR. With this, AIR of up to 424 Gbit/s employing a DP 128 GBd 4 PAM signal has been achieved. While the DP 160 GBd 2 PAM signal offered AIR of 276 Gbit/s, the DP 64 GBd 8 PAM signal achieves AIR of 338 Gbit/s. However, these correspond to best case rates. For reliable implementations one has to consider

outage rates. There it has been shown that it is more effective to operate at a higher system margin to increase effective data rates. This constitutes to the best of our knowledge the highest achieved symbol rate in an FSO communication link. These highest symbol rates have been enabled by a packaged plasmonic modulator offering a 3-dB bandwidth > 110 GHz.

Radiation tests for total ionized doses of 20 and 50 krad (Si) are presented and only minor dose-independent degradations were observed - making plasmonic modulators a future contender for FSO in space.

Lastly, the atmospheric conditions during the measurement timeframe were assessed on-site and are described. It can be seen that the conditions represent a worst-case scenario for GEO-feeder links. High link performance could still be achieved with real-time turbulence mitigation provided by an AO system, which greatly improved the performance during the measurement timeframe.

Acknowledgment

We thank Jungfrau Railways, International Foundation High Altitude Research Stations Jungfraujoch and Cornergrat (HFSJG), Astronomical Institute University Bern (AIUB) for allowing us to conduct the experiments on their premises. We thank skw-logistics, Mr. Pierre Lauber, Arnaud Le Kernec, and Mr. G. Tamburello for their support. The co-authors would like to thank ESA for lending the FEEDELIO equipment developed by ONERA in the framework of ESA's contract N°4000120300/17/NL/PS. The co-authors would like to thank ESA for FEEDELIO (N°4000120300/17/NL/PS). Polariton Technologies acknowledges NLM Photonics for providing the organic electro-optic material.

References

[1] N. Kadowaki et al., "Short TESAT laser communication terminal performance results on 5.6Gbit coherent inter-satellite and satellite to ground links," *Proc. SPIE*, vol. 10565, pp. 324–329, 2010.

[2] M. Toyoshima, "Recent trends in space laser communications for small satellites and constellations," *J. Lightw. Technol.*, vol. 39, no. 3, pp. 693–699, Feb. 2021, doi: 10.1109/jlt.2020.3009505.

[3] V. W. Chan, "Optical space communications," *IEEE J. Sel. Topics Quantum Electron.*, vol. 6, no. 6, pp. 959–975, Nov./Dec. 2000.

[4] F. P. Guiomar, M. A. Fernandes, J. L. Nascimento, V. Rodrigues, and P. P. Monteiro, "Coherent free-space optical communications: Opportunities and challenges," *J. Lightw. Technol.*, vol. 40, no. 10, pp. 3173–3186, May 2022, doi: 10.1109/jlt.2022.3164736.

[5] Y. Horst et al., "Tbit/s line-rate satellite feeder links enabled by coherent modulation and full-adaptive optics," *Light. Sci. Appl.*, vol. 12, no. 1, Jun. 2023, Art. no. 153, doi: 10.1038/s41377-023-01201-7.

[6] P. P. Mitra and J. B. Stark, "Nonlinear limits to the information capacity of optical fibre communications," *Nature*, vol. 411, no. 6841, pp. 1027–1030, 2001.

[7] P.-L. Chen et al., "Demonstration of 16 channels 10 Gb/s WDM free space transmission over 2.16 km," in *Proc. Dig. IEEE/LEOS Summer Topical Meetings*, 2008, pp. 235–236.

[8] E. Ciaramella et al., "1.28 terabit/s (32x40 Gbit/s) WDM transmission system for free space optical communications," *IEEE J. Sel. Areas Commun.*, vol. 27, no. 9, pp. 1639–1645, Dec. 2009, doi: 10.1109/jsac.2009.091213.

[9] J. C. Juarez, D. W. Young, J. E. Sluz, J. L. Riggins II, and D. H. Hughes, "Free-space optical channel propagation tests over a 147-km link," *Proc. SPIE*, vol. 8038, 2011, Art. no. 80380B, doi: 10.1117/12.886890.

[10] J. Poliak, R. M. Calvo, and F. Rein, "Demonstration of 1.72 tbit/s optical data transmission under worst-case turbulence conditions for ground-to-geostationary satellite communications," *IEEE Commun. Lett.*, vol. 22, no. 9, pp. 1818–1821, Sep. 2018.

[11] A. Dochhan, J. Poliak, J. Surof, M. Richerzhagen, H. F. Kelemu, and R. M. Calvo, "13.16 Tbit/s free-space optical transmission over 10.45 km for geostationary satellite feeder-links," in *Proc. 20th ITG-Symp. Photonic Netw.*, 2019, pp. 1–3.

[12] F. P. Guiomar et al., "Adaptive probabilistic shaped modulation for high-capacity free-space optical links," *J. Lightw. Technol.*, vol. 38, no. 23, pp. 6529–6541, Dec. 2020, doi: 10.1109/jlt.2020.3012737.

[13] M. A. Fernandes, P. P. Monteiro, and F. P. Guiomar, "Single-wavelength terabit FSO channel for datacenter interconnects enabled by adaptive PCS," in *Proc. Opt. Fiber Commun. Conf. Exhib.*, 2021, pp. 1–3.

[14] N. Perlot et al., "18km bidirectional free-space optical link with multi-aperture antenna and DWDM SFP+ transceivers (VERTIGO project)," *Proc. SPIE*, vol. 12413, 2023, Art. no. 124130W.

[15] M.-C. Jeong et al., "8 × 10 Gb/s terrestrial optical free space transmission over 3.4 km using an optical repeater," in *Proc. Opt. Fiber Commun. Conf.*, 2002, vol. 70Paper ThD4. [Online]. Available: https://opg.optica.org/abstract.cfm?URI=OFC-2002-ThD4,https://opg.optica.org/abstract.cfm?URI=OFC-2002-ThD4

[16] J. Mukherjee and B. Ramamurthy, "Communication technologies and architectures for space network and interplanetary internet," *IEEE Commun. Surveys Tut.*, vol. 15, no. 2, pp. 881–897, Second Quarter 2013, doi: 10.1109/surv.2012.062612.00134.

[17] R. Mata Calvo et al., "Optical technologies for very high throughput satellite communications," *Proc. SPIE*, vol. 10910, pp. 189–204, 2019.

[18] A. M. Bonnefois et al., "Feasibility demonstration of AO pre-compensation for GEO feeder links in a relevant environment," *Opt Exp.*, vol. 30, no. 26, pp. 47179–47198, Dec. 2022, doi: 10.1364/OE.470705.

[19] A. L. Kernec et al., "The H2020 VERTIGO project towards tbit/s optical feeder links," *Proc. SPIE*, vol. 11852, 2021, Art. no. 1185217.

[20] V. Billault et al., "Optical coherent combining of high-power optical amplifiers for free-space optical communications," *Opt. Lett.*, vol. 48, no. 14, pp. 3649–3652, Jul. 2023, doi: 10.1364/OL.494908.

[21] D. J. Geisler, T. M. Yarnall, M. L. Stevens, C. M. Schieler, B. S. Robinson, and S. A. Hamilton, "Multi-aperture digital coherent combining for free-space optical communication receivers," *Opt. Exp.*, vol. 24, no. 12, pp. 12661–12671, Jun. 2016, doi: 10.1364/OE.24.012661.

[22] H. Hemmati et al., "Experimental demonstration of multi-aperture digital coherent combining over a 3.2-km free-space link," *Proc. SPIE*, vol. 10096, pp. 86–93, 2017.

[23] N. Védrenne et al., "First experimental demonstration of adaptive optics pre-compensation for GEO feeder links in a relevant environment," in *Proc. IEEE Int. Conf. Space Opt. Syst. Appl.*, 2019, pp. 1–5.

[24] A. Montmerle Bonnefois et al., "Adaptive optics pre-compensation for GEO feeder links: The FEEDELIO experiment," *Proc. SPIE*, vol. 1180, 2019, Art. no. 1185217, doi: 10.1117/12.2536003.

[25] N. Védrenne et al., "Performance analysis of an adaptive optics based optical feeder link ground station," *Proc. SPIE*, vol. 11852, pp. 527–535, 2020.

[26] R. Boddeda, D. R. Arrieta, S. Almonacil, J. Renaudier, and S. Bigo, "Achievable capacity of geostationary-ground optical links," *J. Lightw. Technol.*, vol. 41, no. 12, pp. 3717–3725, Jun. 2023, doi: 10.1109/jlt.2023.3271824.

[27] J. Yan, Z. Zheng, W. Hu, and A. Xu, "Improved performance of M-ary PPM free-space optical communication systems in atmospheric turbulence due to forward error correction," in *Proc. Int. Conf. Commun. Technol.*, 2006, pp. 1–4.

[28] L. B. Stotts and L. C. Andrews, "Bit error rate performance of a laser ground-to-satellite uplink communications systems in the presence of atmospheric turbulence and loss," in *Proc. IEEE Int. Conf. Space Opt. Syst. Appl.*, 2022, pp. 66–73.

[29] D. R. Arrieta et al., "Proof-of-concept real-time implementation of interleavers for optical satellite links," *J. Lightw. Technol.*, vol. 41, no. 12, pp. 3932–3942, Jun. 2023, doi: 10.1109/jlt.2023.3270769.

[30] R.-J. Essiambre, G. Kramer, P. J. Winzer, G. J. Foschini, and B. Goebel, "Capacity limits of optical Fiber networks," *J. Lightw. Technol.*, vol. 28, no. 4, pp. 662–701, Feb. 2010, doi: 10.1109/jlt.2009.2039464.

[31] M. Burla et al., "500 GHz plasmonic Mach-Zehnder modulator enabling sub-THz microwave photonics," *APL Photon.*, vol. 4, no. 5, 2019, Art. no. 056106, doi: 10.1063/1.5086868.

[32] L. Kulmer et al., "Plasmonic modulators for future highest-speed free space optical communications," in *Proc. Opt. Fiber Commun. Conf.*, 2023, Paper W3I. 1.

[33] Q. Hu et al., "Ultrahigh-net-bitrate 363 gbit/s PAM-8 and 279 gbit/s polybinary optical transmission using plasmonic Mach-Zehnder modulator," *J. Lightw. Technol.*, vol. 40, no. 10, pp. 3338–3346, May 2022, doi: 10.1109/jlt.2022.3172246.

[34] C. Haffner et al., "All-plasmonic Mach–Zehnder modulator enabling optical high-speed communication at the microscale," *Nature Photon.*, vol. 9, no. 8, pp. 525–528, 2015, doi: 10.1038/nphoton.2015.127.

[35] C. E. Jordan, "NASA radiation belt models AP-8 and AE-8," RADEX INC BEDFORD MA, 1989.

[36] S. M. Seltzer, "Updated calculations for routine space-shielding radiation dose estimates: SHIELDOSE-2," NIST Publication NISTIR, vol. 5477, 1994.

[37] D. Heynderickx, B. Quaghebeur, E. Speelman, and E. Daly, "Short ESA's Space Environment Information System (SPENVIS) - A WWW interface to models of the space environment and its effects," in *Proc. 38th Aerosp. Sci. Meeting Exhib.*, 2000.

[38] E. W. Taylor et al., "Radiation resistance of electro-optic polymer-based modulators," *Appl. Phys. Lett.*, vol. 86, no. 20, 2005, Art. no. 201122.

[39] P. Habegger et al., "Plasmonic 100-GHz electro-optic modulators for cryogenic applications," in *Proc. ECOC*, 2022, Paper Tu1G.1.

[40] M. Eppenberger et al., "Resonant plasmonic micro-racetrack modulators with high bandwidth and high temperature tolerance," *Nature Photon.*, vol. 17, pp. 360–367, 2023, doi: 10.1038/s41566-023-01161-9.

[41] D. L. Fried, "Optical resolution through a randomly inhomogeneous medium for very long and very short exposures," *JOSA*, vol. 56, no. 10, pp. 1372–1379, 1966.

[42] T. Fusco et al., "NAOS on-line characterization of turbulence parameters and adaptive optics performance," *J. Opt. A: Pure Appl. Opt.*, vol. 6, no. 6, pp. 585–596, 2004, doi: 10.1088/1464-4258/6/6/014.